ADVANCED OPTICAL MATERIALS
www.advopticalmat.de

Ligand-Induced Crystallization Control in $MAPbBr_3$ Hybrid Perovskites for High Quality Nanostructured Films

*Markus W. Heindl, Michael F. Lichtenegger, Tim Kodalle, Shangpu Liu, Nasrin Solhtalab, Jonathan Zerhoch, Andrii Shcherbakov, Milan Kivala, Carolin M. Sutter-Fella, Alexander S. Urban, and Felix Deschler**

Controlling the formation of hybrid perovskite thin films is crucial in obtaining high-performance optoelectronic devices, since factors like morphology and film thickness have a profound impact on a film's functionality. For light-emitting applications grain sizes in the sub-micrometer-range have previously shown enhanced brightness. It is therefore crucial to develop simple, yet reliable methods to produce such films. Here, a solution-based synthesis protocol for the on-substrate formation of $MAPbBr_3$ (MA = methylammonium) nanostructures by adding the bifunctional *rac*-3-aminobutyric acid to the precursor solution is reported. This synthesis route improves key optical properties such as photoluminescence quantum yields and life times of excited states by inducing a controlled slow-down of the film formation and suppressing agglomeration effects. In situ spectroscopy reveals a delayed and slowed down crystallization process, which achieves synthesis of perovskite structures with much reduced defect densities. Further, aggregation can be controlled by the amount of amino acid added and adjusting the synthesis protocol allows to produce cubic crystallites with targeted size from nanometer to micrometer scales. The nanocrystalline $MAPbBr_3$ samples show enhanced amplified spontaneous emission (ASE) intensities, reduced ASE thresholds and purer ASE signals, compared to pristine films, even under intense optical driving, making them promising structures for lasing applications.

1. Introduction

Over the recent years lead-halide perovskites with the chemical structure $APbX_3$ (A = methylammonium (MA^+), formamidinium (FA^+) or cesium (Cs^+), X = Cl^-, Br^-, I^- or a mixture of these) have been demonstrated to hold great promise for optical devices, particularly because they allow for an uncomplicated fabrication via solution processing. A key take-away from the rapid advance in research on these materials is that synthetic control over the morphology of thin films is essential for the performance of any device made from them.[1,2] In general terms, large crystalline domains with bulk or bulk-like properties enable long carrier diffusion lengths, which, combined with 3D bulk perovskite's low exciton binding energy and broad absorption range, have enabled the design of high-performing solar cells.[3,4] On the other hand, when building efficient emitters like LEDs or lasers, promoting the generation of excitons has been proven

M. W. Heindl, S. Liu, N. Solhtalab, J. Zerhoch, A. Shcherbakov, F. Deschler
Institute for Physical Chemistry
Heidelberg University
Im Neuenheimer Feld 229, 69120 Heidelberg, Germany
E-mail: felix.deschler@pci.uni-heidelberg.de
M. W. Heindl, S. Liu, J. Zerhoch, A. Shcherbakov
Walter Schottky Institute
Technical University of Munich
Am Coulombwall 4, 85748 Garching, Germany

The ORCID identification number(s) for the author(s) of this article can be found under https://doi.org/10.1002/adom.202402441

DOI: 10.1002/adom.202402441

M. W. Heindl, S. Liu, J. Zerhoch, A. Shcherbakov
Physics Department, TUM School of Natural Sciences
Technical University of Munich
85748 Garching, Germany
M. F. Lichtenegger, A. S. Urban
Nanospectroscopy Group and Center for Nanoscience (CeNS)
Nano-Institute Munich, Department of Physics
Ludwig-Maximilians-Universität München
Königinstr. 10, 80539 Munich, Germany
T. Kodalle, C. M. Sutter-Fella
Molecular Foundry
Lawrence Berkeley National Laboratory
1 Cyclotron Rd., Berkeley, California 94720, USA
T. Kodalle
Advanced Light Source
Lawrence Berkeley National Laboratory
1 Cyclotron Rd., Berkeley, California 94720, USA
M. Kivala
Institute of Organic Chemistry
Heidelberg University
Im Neuenheimer Feld 270, 69120 Heidelberg, Germany

an efficient strategy. This can for instance be achieved by the segmentation of perovskite thin films into nanometer-scaled grains, which in turn increases radiative recombination rates through special confinement of the involved charge carriers.[2,4–6]

The perhaps best known example for such improvements through size reduction are colloidal perovskite quantum dots which have been shown to display remarkably high quantum yields.[7] However, since these kinds of nanocrystals (NCs) are synthesized ex-situ they require post-synthesis purification and further processing, e.g. to remove the long, electrically isolating ligands, a process which introduces defects and causes agglomeration, diminishing the final device performance.[2,4,8,9] Another promising approach for producing perovskite thin films with bright emission therefore appears to be the direct formation of nano- and sub-micrometer-structures on a substrate, typically referred to as in situ synthesis. For this, two general strategies exist. First, the perovskites can be synthesized within a porous matrix as for example a polymer or silica.[10] While this approach allows for the desired size control, the presence of a matrix structure is bound to cause issues with electric contacting. Alternatively, perovskite NCs can be produced in situ via ligand engineering.[8,11] This approach can be compared to the ligand assisted reprecipitation in colloidal chemistry.[12] The addition of an antisolvent during the spin coating process forces the instant supersaturation of the perovskite precursor solution resulting in the imminent formation of multiple seed crystals whose' agglomeration is suppressed via added organic ligands or alternatively an excess of the A-site cation.[4,8,11,13] The benefits of this method are that it allows for the use of much shorter ligands than colloidal approaches and that post-synthesis treatment is not necessarily required, even though some methods have been shown to further improve the obtained results.[4,8,14] However, the use of an antisolvent also comes with certain downsides as the rather rapid nature of the reaction results in poor shape control and internal strain effects.[8,13,15]

Here, we report a novel approach to the antisolvent-free in situ fabrication of perovskite micrometer- and sub-micrometer-structures via ligand engineering. We utilize an amino acid to act both as spacer preventing agglomeration and as delaying agent slowing down the film formation to allow for the controlled synthesis of low-defect perovskite thin films. This innovative method represents a novel strategy for the fabrication of micrometer and sub-micrometer structures. Utilizing organic additives to slow down the crystallization process allows to achieve reaction kinetics more similar to those usually used for much larger structures, e.g. in the synthesis of single crystals via controlled temperature lowering. The result are high quality crystals with defined shapes, predetermined scale and reduced defect densities, leading to significantly improved optical properties such as higher photoluminescence quantum yields (PLQY) and more energy efficient amplification by spontaneous emission (ASE), an optical effect that has received significant scientific attention as it represents a prestep to the construction of a laser device.[16,17] Importantly, this synthesis takes place on substrate, allowing for imminent processing without the need for additional purification or deposition steps, making this a promising strategy for the fabrication of optoelectronic devices.

2. Results and Discussion

Amino acids are generally characterized as small organic molecules displaying both a carboxyl and an amino functional group. Via an intramolecular proton transfer between these two building blocks, they are able to form internal salts which display both a positive and a negative electric charge while remaining an overall neutral molecule. This enables them to effectively bind to the surfaces of perovskites and related structures, a fact that has been exploited for surface passivation, the imprinting of chiral information and the stabilization of colloidal dispersions.[18,19,20] In regards to the in situ fabrication of nanometer-scaled perovskite structures, amino acids have been shown to enable the fabrication of such materials via a simple process based on spin-coating and subsequent annealing, either directly or through combination with other organic spacer cations.[21,22]

Based on these results we mix the amino acid *rac*-3-aminobutyric acid (3-ABA) with the precursors for the green-light emitting perovskite $MAPbBr_3$. Since a small excess of the MA-cation has been shown to improve luminescence properties by suppressing the formation of metallic lead, we chose a ratio of 3-ABA to $PbBr_2$ to MABr of 1:1:1.05.[23] The prepared mixture is dissolved in DMSO at 100 °C to form a clear 0.5 M solution. We note this as an important observation since pure 3-ABA does not dissolve in DMSO under the same conditions (see Figure S1 in the Supporting Information). Similar changes of solubility in the presence of metal ions have been linked to the formation of metal-organic complexes, which is also a likely explanation here.[24] While the interactions between amino acids and finished perovskite interfaces are usually described as hydrogen bonds, such a precursor-complex could potentially be of more covalent nature, for instance with the Pb^{2+} cation acting as a Lewis acid.[22,25]

Since the spin-coating of a hot solution may result in issues with reproducibility due to its ongoing cooling process, the precursor solution is allowed to cool to room temperature over two hours, during which no precipitation was observed. Then the 3-ABA containing mix is spin-coated for 40s and afterwards instantly annealed (also see Experimental Section). As shown in Figure S2 (Supporting Information), the sample obtained this way displays an improved PLQY of 1.76% compared to 0.26% for pure $MAPbBr_3$ without the addition of 3-ABA (for more information on the PLQY measurements see Table S1 in the Supporting Information). This represents an impressive, almost 7-fold increase in efficiency.

To better understand the origins of this improvement, we conduct further experiments to investigate why pristine $MAPbBr_3$ appears fully formed after spin-coating while the film containing 3-ABA only appears during the subsequent annealing step, indicating a difference in the formation process that goes beyond surface passivation. To study this, we deviate from the established instant annealing (IA) approach and allowed the sample to rest for 45 minutes before annealing – a value chosen as a trade-off between performance and time-efficient fabrication (see Figure S3 in the Supporting Information). This increased the PLQY even further to 7.3% after annealing, 4 times higher than for fabrication that uses the IA approach. This is despite the limitations to external quantum yields associated with internal

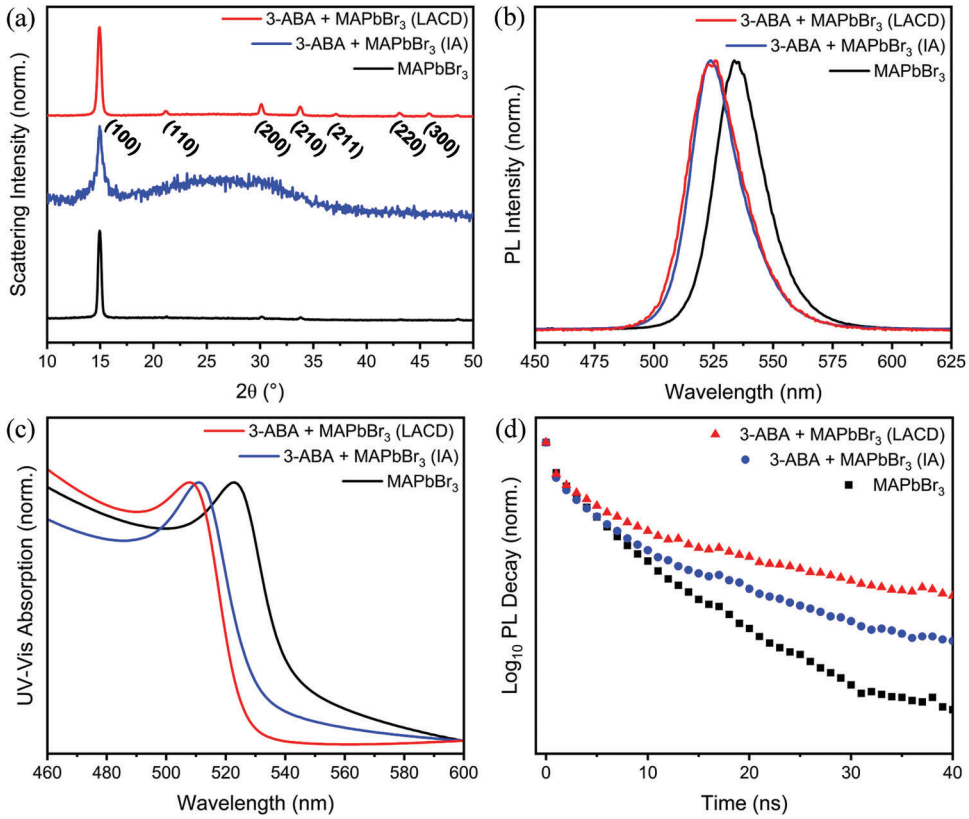

Figure 1. Structural and optical properties of pristine $MAPbBr_3$ (black), instantly annealed $MAPbBr_3$ with added 3-ABA at a 1:1 ratio (blue) and 3-ABA modified $MAPbBr_3$ (1:1 ratio) prepared according to the LACD protocol (red). a) XRD data proves the formation of $MAPbBr_3$ thin films in all three cases, even though crystallinity is significantly reduced for the instantly annealed sample. Miller indices are listed below the respective reflexes of the LACD sample.[29] Both samples containing 3-ABA display a blue-shift in their b) PL and c) absorption data. The steeper rise of intensity in the absorption data also indicates reduced scattering in the sample fabricating according to the LACD protocol. d) TRPL measurements at 400 nm and a fluence of 13.2 μJ cm^{-2} show that the addition of 3-ABA can significantly enhance PL lifetime in $MAPbBr_3$ samples. This effect is especially pronounced when using the LACD approach for sample fabrication.

reflection phenomena in plane perovskite films.[26] We will refer to this method as ligand-assisted crystallization delay (LACD), the exact mechanism of which will be discussed below. The detailed PLQY data can be found in Table S1 (Supporting Information). The described differences in quantum yield affect the films' brightness which can be seen by eye using a UV-Lamp and is largely independent of annealing times (see Figure S4 in the Supporting Information).

The structural properties of unmodified $MAPbBr_3$ are studied by X-ray diffraction (XRD). The recorded diffractogram is dominated by the (100) reflex at 14.95° (see **Figure 1**a, black curve). Similarly, films prepared after the addition of 3-ABA via the IA method also display a clearly visible (100) reflex indicating the formation of $MAPbBr_3$ (see Figure 1a, blue curve).[27] However, the signal-to-noise ratio has deteriorated significantly for this sample, indicating a reduction in crystallinity. In contrast, if the perovskite films are prepared with 3-ABA utilizing the LACD method, the obtained diffractograms are much less noisy and even smaller reflexes at higher angles are clearly visible (see Figure 1a, red curve). We attribute this to an increase in crystallinity compared to the IA method and a reduction of preferred orientation when compared to unmodified $MAPbBr_3$. The latter is thereby confirmed by grazing incident wide angle X-ray scattering (GIWAXS), where the (100) signal appears significantly broader for the LACD sample (see Figure S5 in the Supporting Information).

In regard to its optical properties, both samples containing 3-ABA exhibit slightly blue-shifted photoluminescence (PL) and absorption spectra (see Figure 1b,c respectively) compared to untreated $MAPbBr_3$. Similar observations have been linked to surface passivation effects and changes in the dielectric environment, which could occur here due to the binding of the amino acid to the perovskite surface.[28] Further, the normalized absorption spectra display differences in signal shape. While the LACD sample displays a flat background and a sharp rise directly before the excitonic peak, the other two samples rise more slowly and show stronger absorption before the excitonic peak is reached, indicating contributions from scattering effects. It can hence be concluded that LACD produces smoother films. Further, our results indicate that the presence of 3-ABA also improves the films' photostability (see Figure S6 in the Supporting Information).

Lifetimes of excited states are probed by time-resolved PL spectroscopy (TRPL). As displayed in Figure 1d, unmodified $MAPbBr_3$ displays relatively short lifetimes, while the addition of 3-ABA via the IA method causes a significant extension of lifetimes, likely due to surface passivation effects that reduce

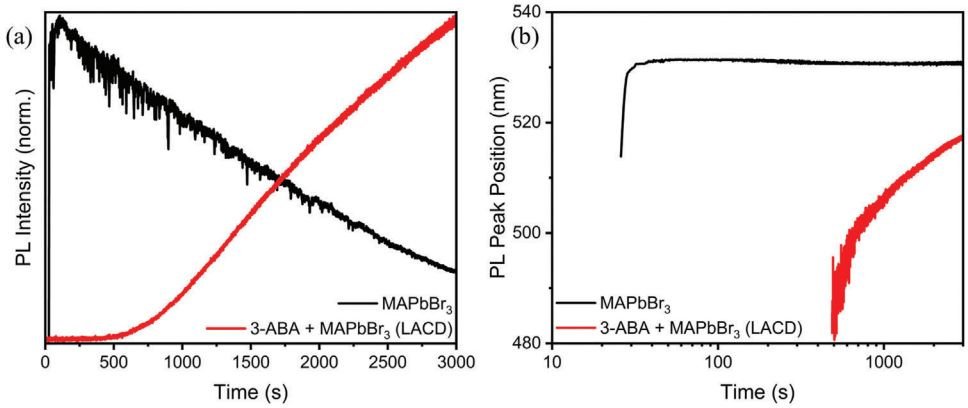

Figure 2. In situ PL for pristine $MAPbBr_3$ (black) and $MAPbBr_3$ with added 3-ABA (1:1 ratio, red). a) Integrated PL emission measured during $MAPbBr_3$ growth. Unmodified $MAPbBr_3$ forms already after ≈26 s. After this the PL intensity of the sample slowly decreases over time, most likely due to beam damage effects. When 3-ABA is added, PL is observed delayed, becoming visible only after more than 6 min. Further, with 3-ABA, PL keeps increasing during the observed timeframe. b) Position of maximum PL intensity. For pristine $MAPbBr_3$ the maximum PL position is constant over the entire time. If 3-ABA is added the PL shifts to higher wavelengths over time.

nonradiative decay processes by lowering the amount of surface defects.[19] However, if 3-ABA is added via the LACD method, lifetimes are even higher than with the IA approach, pointing towards an additional reduction of defects beyond surface passivation. These observations are consistent for all investigated fluences (see Figure S7 in the Supporting Information) and agree well with the observed trend of increased PLQY upon adding the amino acid.

We investigate the film formation by utilizing in situ PL spectroscopy to better understand the origin of these differences. Here, the luminescent properties of the sample are constantly probed with a 405 nm laser during spin-coating and the subsequent waiting period and the integrated PL intensity and the position of the highest signal intensity are plotted in **Figure 2**. For pristine $MAPbBr_3$ the crystallization begins after about 26 s, well within the 40 s of spin-coating, as seen in Figure 2a (black line). In accordance with literature observations, the initial crystallization process occurs fast, which is indicated by a significant increase in PL intensity within a few seconds (see Figure S8a in the Supporting Information).[30] During the subsequent waiting period at room temperature, the PL intensity slowly decreases over time. While some early decrease of PL intensity is expected due to agglomeration of perovskite crystallites,[31] this probably is mostly a result of beam damage and/or local laser-induced heating effects leading to phonon-assisted nonradiative recombination and not a part of the formation process itself.[32] However, it is worth noting that the position of the PL peak remains unchanged after the 40s spin-coating process has concluded (see Figure 2b, black line).

In contrast, a sample that was modified with 3-ABA displays no PL during the spin coating process of 40 s but instead takes about 6 min for a signal to appear and start slowly rising (see Figure 2a, red line and Figure S9 in the Supporting Information). This time span can be decreased by reducing the amount of 3-ABA added to the precursor solution (see Figure S10 in the Supporting Information). We conclude that 3-ABA is able to delay the crystallization process, potentially due to the formation of the before mentioned metal-organic complex that may bind Pb^{2+} cations, which hence are unavailable to form $MAPbBr_3$. In other words, the 3-ABA could "store" Pb^{2+} in form of a highly solvable complex and consequently prevent the solution from reaching the critical concentration required to begin the nucleation of perovskite-crystallites during the spin-coating process. This postulated system can be described via a chemical equilibrium approach as detailed in Scheme S1 (Supporting Information). As a result, the main crystallization phase is also slowed down significantly, taking several minutes with 3-ABA in contrast to just a few seconds in the case without 3-ABA. The slower LACD approach can therefore perhaps be compared to the synthesis of single crystals via a temperature lowering approach.[33] Slowing down the crystal growth generally can help to eliminate crystallization defects and thereby partly explain the increases in PLQY, PL lifetimes and crystallinity.[34] Annealing the still wet film, as done during the IA method, evaporates the solvent faster and thereby negates this effect. Hence, in Figure S11 (Supporting Information) a PL signal is observed only seconds after placing a 3-ABA film on a hotplate.

Unlike for the pure $MAPbBr_3$ sample, the position of the PL emission peak does not stay constant during the waiting period when using the LACD method. Instead, a slow but constant red-shift can be observed (see Figure 2b, red line). This observation supports the hypothesis of a much slower growth of perovskite crystals. The initially formed perovskite nuclei display a blue-shifted PL, either though band-gap altering defects that are eliminated over time or due to size-dependent quantum confinement, an effect that due to their ongoing growth is slowly reduced until the crystallites exceed the minimum size required for noticeable confinement effects.[31,35] It should be noted that the same effect can be observed in pristine $MAPbBr_3$, however it is already negligible after a few seconds during the spin-coating process (see Figure 2b, black line and Figure S8b in the Supporting Information), indicating that a similar process takes places without added 3-ABA and hence pointing towards a size-based explanation.

However, the growth of perovskite crystals is not solely dependent on the availability of dissolved precursor ions. Coalescence effects can also play an important role in these formation processes.[36] Given the observed slower red-shift of the PL in

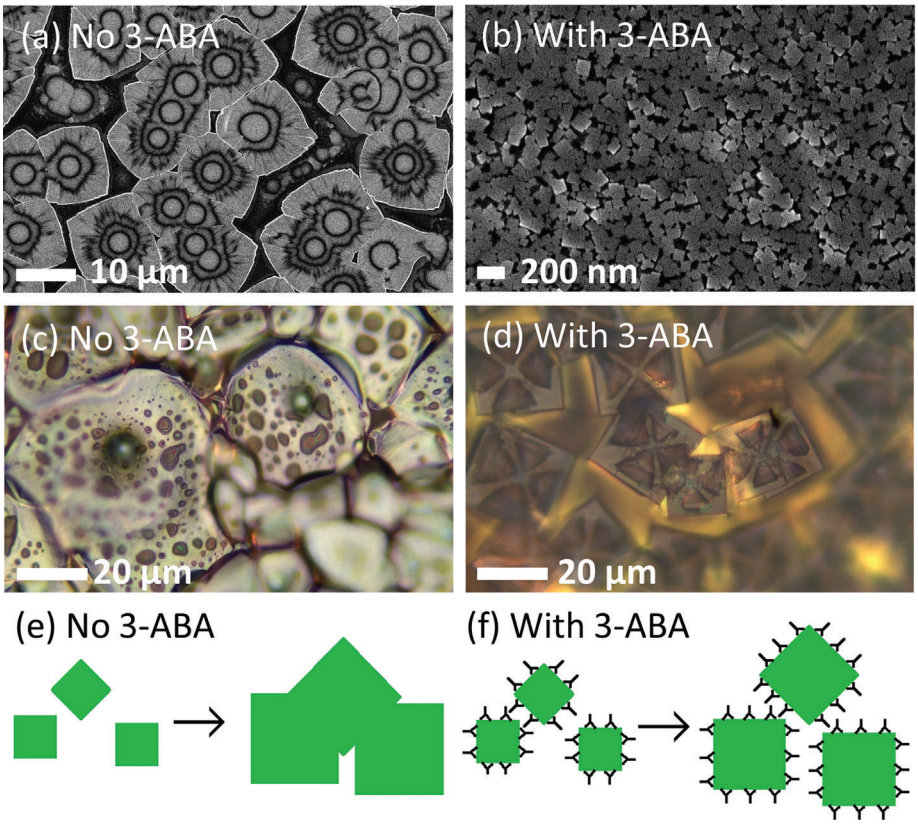

Figure 3. a) SEM-based imaging reveals that pristine $MAPbBr_3$ forms as large, oddly shaped crystallites with a size in the 10 µm range. b) If $MAPbBr_3$ is spin-coated with 3-ABA (1:1 ratio) according to the LACD method, the resulting crystals are significantly smaller, in the range between 25 and 100 nm. Additionally, the crystals' edges are well defined and their cubic shapes are mostly visible. c) Drop-Casting pristine $MAPbBr_3$ leads to similarly odd shapes as the spin-casting approach, as revealed by optical microscopy. d) However, if the sample is drop-casted with added 3-ABA (1:1 ratio), the formed crystals are clearly of cubic shape. We attribute this to the ability of 3-ABA to suppress the agglomeration of crystallites during the growth process. e) Without this additive, early stage nuclei combine to larger crystals, losing their originally cubic shape. f) 3-ABA surface ligands are able to prevent this by binding to the nucleis' surfaces and hence preserve the crystals' cubic shape.

presence of 3-ABA which indicates reduced growth of $MAPbBr_3$ crystallites, it is worth considering if these kind of agglomeration effects are also being suppressed by the organic additive. As amino acids have already been used as organic spacers to stabilize perovskite NCs, this seems like a probable scenario.[20,22,37] Looking at the film morphologies by scanning electron microscopy (SEM), we can confirm this hypothesis. While spin-coated pristine $MAPbBr_3$ forms large crystallites in the ten-micrometer-range (see **Figure** 3a), the fabrication with LACD results in significantly smaller domains of about 25–100 nm and – in agreement with the GIWAXS data shown in Figure S5 – an apparently more random distribution of crystal orientation facilitated through the organic additive (see Figure 3b). Further, it appears that this fabrication technique also results in cubic crystallites. As this crystal shape matches the crystal structure of $MAPbBr_3$, this observation indicates isotropic growth.[38] This likely originates from a slow and controlled crystallization process that – as seen in the results of our in situ measurements displayed in Figure 2a – does not display a step of strong increase of PL intensity in a short time frame.

The crystal sizes observed in SEM are also underpinned by analyzing GIWAXS data via the Scherrer equation, which can be used to determine a lower boundary for crystalline domain sizes.[39,40] While these measurements indicate some lateral inhomogeneities, the obtained sizes of 25–45 nm are in good agreement with the smaller crystallites observed in the SEM, supporting the theory of monolithic growth of individual crystals. This kind of shape-control when fabricating perovskite nanostructures in situ is difficult to achieve through fast, anti-solvent-based methods, again highlighting the role of the slowed-down formation process. Other studies have also achieved similarly well-defined crystal shapes by decelerating formation dynamics. However, usually this was done with specialized equipment like polymer masks to restrict evaporation, setups for heating alternating substrate areas or specialized diffusion chambers that allow for the ultraslow addition of anti-solvents, adding an additional layer of complexity not required in our approach.[41]

To test the ability of 3-ABA to suppress agglomeration effects, we prepared additional samples by drop-casting the previously described precursor solutions instead of spin-coating them. Again, pristine $MAPbBr_3$ crystallizes in undefined shapes displayed in Figure 3 via optical microscopy. In contrast, drop-casted films containing 3-ABA form cubic crystals with remarkably straight edges (see Figure 3d). This demonstrates the ability of 3-ABA to suppress agglomeration, both on the nano- and micrometer-scale. Without its moderation, early-stage crystallites

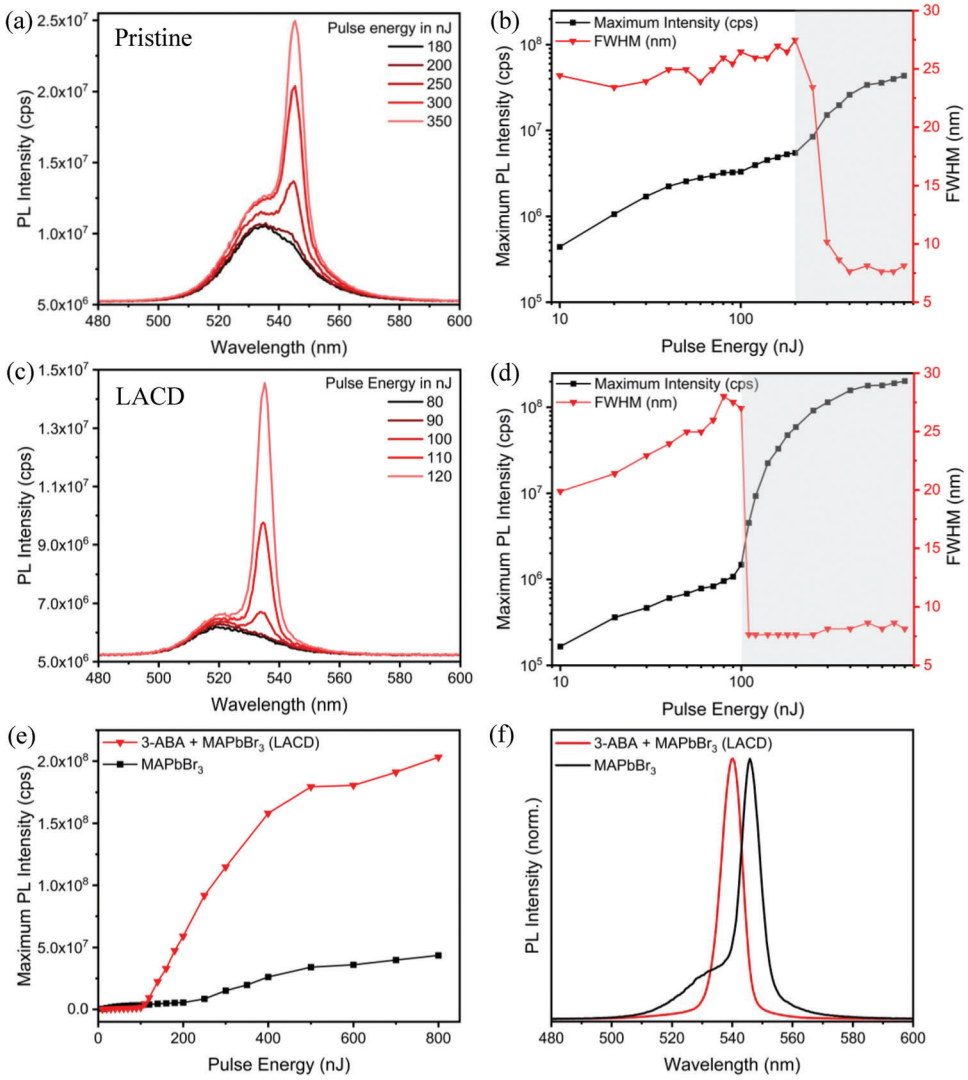

Figure 4. Luminescence properties of $MAPbBr_3$ with and without added 3-ABA depending on excitation pulse energy. a) Pristine $MAPbBr_3$ begins to show an extra peak associated with ASE at an excitation pulse energy of 200 nJ. This peak's intensity shows a stronger increase with pulse energy than regular PL. b) The resulting trend shows a sudden drop FWHM at this point and a stronger increase of intensity before leveling off due to saturation effects. Areas in which ASE occurs are highlighted. c) For $MAPbBr_3$ fabricated based on the LACD method and a $PbBr_2$ to 3-ABA ratio of 1:1, ASE effects become visible at even lower pulse energies. d) Accordingly, both the drop in FWHM and the stronger increase of PL are observed earlier. e) We further observe significantly stronger overall ASE intensity for the LACD sample at high pulse energies. f) This can be explained by a comparison of the spectra of both samples at an excitation pulse energy of 800 nJ which shows that pristine $MAPbBr_3$ still displays a combination of its regular PL and ASE while for the LACD sample the ASE signal dominates, indicating more efficient amplification for the later material. This results in a significantly stronger overall ASE intensity for the LACD sample at high pulse energies. The blue shift of the LACD ASE originates from the blue shift of the PL signal as discussed above.

combine randomly resulting in a loss of their original cubic form, as illustrated in Figure 3e. However, when 3-ABA is present, it can bind to the surface of perovskite crystals and act as a spacer that prevents agglomeration (see Figure 3f), an ability that is most likely based on the reportedly strong binding of amino acids to perovskite surfaces.[22]

In the following we will demonstrate the benefits of samples fabricated via LACD by using them for ASE studies, a prestage for the development of laser devices.[42] For this, the films are excited with a pulsed laser with increasing power until population inversion is achieved.[43] At this point, the films begin to display enhanced, narrow emission. For pristine $MAPbBr_3$ this occurs at a pulse energy of 200 nJ (or a fluence of ≈63.8 μJ cm^{-2}), as shown in **Figure 4**a. Upon further increase of the laser intensity the combined signal's FWHM drops significantly while the intensity of the emission with excitation power becomes steeper, a clear sign of ASE (see Figure 4b). Ultimately, at high fluences, the emission intensity begins to level off.

For samples prepared with LACD a similar overall trend is observed. However, comparing the pre-ASE FWHM values of both samples, the 3-ABA modified sample displays a smaller value at low fluences, indicating a reduction of defects.[44] With increased

fluence this value approaches the one of pristine $MAPbBr_3$, indicating a stronger dependency on heating effects, perhaps due to the smaller grain size that may limit cooling. Further, in the sample containing 3-ABA the ASE threshold is significantly reduced by around half to 100 nJ (or ≈31.9 µJ cm^{-2}), as seen in Figure 4c. This can be explained by how the grain size determines the type of excited state that is photogenerated by optical excitation in the film.[5] For polycrystalline samples with large grains, at low fluences mostly free charge carriers are generated and only for higher fluences excitons become the dominant species of excited states. In contrast, for smaller crystallites in the ≈50 nm range, comparable to those fabricated by LACD, photoexcitation always results in the prevalent generation of excitons, independent of fluence, which is at least partly due to a higher exciton binding energy for smaller crystals.[5,45] Based on these results, control of crystallite size, as presented in this work, is a key parameter in reducing ASE thresholds as the spatial confinement of charge carriers results in an increased excitonic character and hence improves radiative recombination.[5,6] For films with a 1:1 ratio of 3-ABA to $PbBr_2$ the observed well-defined cubic crystal shapes could also contribute to the reduction in ASE thresholds. Here, individual crystals could be acting as micro cavities based on their relatively smooth surfaces, potentially resulting in local whispering-gallery mode lasing at low fluences.[46] Samples fabricated via the LACD approach also display a steeper increase in intensity (see Figure 4d), meaning that ASE does not only occur at lower energies compared to $MAPbBr_3$ but also with a higher overall efficiency.

It should further be noted that the lowest observed ASE threshold did not occur in samples with a 1:1 ratio of 3-ABA to lead but rather in the ones with a 0.75:1 ratio (see Figure S12 in the Supporting Information). Here, ASE could be observed at only 80 nJ pulse energy or a fluence of ≈25.5 µJ cm^{-2}, placing it in a similar range as other state-of-the-art, solution-processed lead-halide perovskite ASE materials, e.g. by Wang et al., who utilized solvent engineering to reduce ASE thresholds in $MAPbBr_3$ from 60 to 21 µJ cm^{-2}.[17] We attribute the observation of low-energy ASE to enhancement effects based on internal scattering.[47] Samples at 75% 3-ABA hence display the ideal mix of morphological disorder and high PLQY (see also Figure S2 in the Supporting Information). Samples prepared with the IA method display a lasing threshold of 180 nJ, located between the untreated $MAPbBr_3$ and the LACD sample (see Figure S13 in the Supporting Information). Most ASE thresholds for perovskite thin films reported in the literature are placed in an order of magnitude from 10^1 to 10^3 µJ cm^{-2}. Since our results are located at the lower end of this range, the utilized LACD fabrication protocol appears to be promising candidate for further research. However, given the large amount of synthetic strategies and excitation parameters that may impact ASE performance, the dedicated reader is referred to the following review articles for a more detailed analysis.[43,48]

Additionally, the peak intensities of samples fabricated according to the LACD protocol were almost two orders of magnitude higher than the ones of unmodified $MAPbBr_3$, as seen in Figure 4e. We attribute this to a much more efficient ASE process in the samples prepared by LACD that allows for a more complete utilization of excited states. This is visible from the recorded emission spectra in Figure 4f. Here, unmodified $MAPbBr_3$ displays a mixture of the sharp ASE signal and the broad peak related to regular spontaneous emission. The latter indicates that not all excited states are contributing to the ASE process. Since this process usually occurs within a few picoseconds after excitation, it is unlikely that this is outcompeted locally by other processes.[49] Thus, most likely there are grains in which ASE never occurs and in which photoexcited states are still affected by the usual nonradiative losses. In contrast, at the same fluence the LACD sample does not display a significant contribution of nonstimulated emission and mostly consists of the ASE signal. This indicates that more excited states are utilized for ASE and do not have the chance to decay nonradiantly, explaining the increase in peak intensity compared to untreated $MAPbBr_3$.

3. Conclusion

In summary, we developed a novel approach for fabricating bright thin films of the hybrid lead halide perovskite $MAPbBr_3$ based on the bifunctional amino acid 3-ABA and provided valuable insights into the underlying reaction mechanism. In situ PL measurements indicate that the additive is able to slow down the crystallization process and thereby reduce the density of defects. Simultaneously, SEM and optical microscopy images imply that 3-ABA is also able to prevent crystallites from agglomerating, enabling the synthesis of cubic perovskite structures, both on the micrometer- and sub-micrometer scale, depending on the chosen method of deposition. The result is a highly crystalline thin film with significantly improved optical properties for light generation, including enhanced PLQY-values and excited state lifetimes. We further demonstrate that these films can be utilized for energy efficient ASE since they display both lower ASE thresholds and higher peak emission intensities than pristine $MAPbBr_3$.

More generally, this work represents a promising proof of concept for a novel approach in the on-substrate fabrication of micrometer and sub-micrometer crystals by controlling crystallization dynamics and the resulting morphologies through organic additives. It further demonstrates that the delay time between spin-coating and annealing can be an important parameter that should always be considered when optimizing fabrication processes for perovskite thin films. We hence believe that this strategy holds great promise for both the fabrication of light emitting devices and fundamental research in early stage crystallization mechanics

4. Experimental Section

Materials: 3-Aminobutyric acid (97%), Lead(II) bromide (≥ 98%) and Dimethyl sulfoxide (DMSO, anhydrous, ≥99.9%) were purchased from Sigma-Aldrich, Methylamine Hydrobromide (>98%) from Tokyo Chemical Industry. All chemicals were used without further purification. Before deposition, all glass substrates were cleaned with isopropanol, blown dry and treated with oxygen plasma.

Sample Preparation: For pristine $MAPbBr_3$, 0.1835 g $PbBr_2$ (0.5 mmol) and 0.0588 g MABr (0.55 mmol) were placed in a glass container. For modified samples, 0.0516 g of 3-ABA (0.5 mmol) was also added. These precursors were dissolved in 1 mL of DMSO by stirring for 1 h at 100 °C. The resulting solution is allowed to cool down for 2 h and subsequently filtered with a PTFE syringe filter (0.2 µm pore diameter). Afterwards, thin films were fabricated by spin-coating 80 µL of precursor solution on a glass

substrate for 40 s at 6000 rpm. The resulting samples were either annealed at 60 °C immediately or let sit for 45 min before annealing at 60 °C for at least 5 min. Samples containing 3-ABA fabricated based on the IA approached were annealed longer to ensure complete crystallization despite any delay effects and hence ensure comparability (see also Figure S4 in the Supporting Information). All fabrication steps were performed under an inert N_2 atmosphere.

Optical Characterization: PL, TRPL and ASE-measurements were all performed utilizing an inhouse build setup based on a *PHAROS* Yb:YAG laser system (Light Conversion), an *ORPHEUS + LYRA* optical parametric amplifier (both Light Conversion) and an *iStar* CCD camera (Andor). The excitation was set to a wavelength of 400 nm and a repetition rate of 5 kHz. The beam power was regulated with a continuously variable neutral density filter. The beam area during ASE measurements was determined as ~0.31 mm^2 while the pulse width was about 40 fs.

UV-Vis absorption spectroscopy was performed with a *Cary 5000* UV–Vis–NIR-Spectrophotometer (Agilent Technologies). PLQE values were determined using a FP-8500 Spectrofluorometer (Jasco).

Structural Characterization: XRD patterns were recorded by a *SmartLab* X-ray diffractometer (Rigaku), using Cu Kα radiation source. GIWAXS data was acquired at beamline 12.3.2 at the Advanced Light Source. The X-ray beam energy was set to 10 keV with an incidence angle of 1°. The GIWAXS signal was detected using a Pilatus 1M 2D detector (Dectris Ltd.) at a sample to detector distance of about 155 mm and an angle of 35°. The data was calibrated using an Al_2O_3 reference sample. Scherrer analysis was performed based on integrated GIWAXS data for the (100) reflex. The X-ray wavelength was 0.124 nm and the shape factor K was assumed as 0.9.[39,50] Measured FWHM were corrected for beam divergence (0.0017 nm) and the energy bandwidth (0.0001 nm) according to Sidhik et al.[50]

In Situ Measurements: In situ PL spectroscopy was performed using a custom-made setup in a nitrogen-filled glove-box. The system is equipped with a 405 nm diode laser as excitation source (Thorlabs) and the PL signal is collected via an optical fiber and recorded using a QEPro spectrometer from Ocean Insights.

Imaging: Optical microscopy was performed with an *inVia* confocal microscopy setup (Renishaw). Scanning electron microscopy (SEM) images of all samples were recorded using a ZEISS SEM Ultra Plus with an acceleration voltage of 3 kV and a FEI Helios 660 operated at 3 kV using immersion mode

Supporting Information

Supporting Information is available from the Wiley Online Library or from the author.

Acknowledgements

M.W.H., S.L., N.S., J.Z., and F.D. acknowledge financial support from the European Research Council (ERC Starting Grant agreement no. 852084 – TWIST). M. W. H., C. M. S.-F. and F.D. recognize the support of the Bavaria California Technology Center (BaCaTec Foerderprojekt Nr 11 [2020-02]). T.K. acknowledges funding by the US Department of Energy (DOE), Office of Science, Office of Basic Energy Sciences, Materials Sciences and Enginnering Division, under contract no. DE-AC02-05CH11231 (D2S2 program KCD2S2). This research used resources of the Advanced Light Source, which is a DOE Office of Science User Facility under contract no. DE-AC02-05CH11231. Specifically, Beamline 12.3.2 was used. Work at the Molecular Foundry was supported by the Office of Science, Office of Basic Energy Sciences, of the U.S. Department of Energy under Contract No. DE-AC02-05CH11231. S. L. acknowledges the financial support from China Scholarship Council (CSC). A.S. acknowledges financial support from the Deutsche Forschungsgemeinschaft (DFG) under the Emmy Noether Program (Project 387651688).

Open access funding enabled and organized by Projekt DEAL.

Conflict of Interest

The authors declare no conflict of interest.

Data Availability Statement

The data that support the findings of this study are openly available in heiDATA at https://doi.org/10.11588/data/C7GKR8.

Keywords

bright, in situ growth, in situ spectroscopy, perovskite nanostructures, stimulated emission

Received: September 9, 2024
Revised: December 29, 2024
Published online: February 5, 2025

[1] a) Y. Li, L. Ji, R. Liu, C. Zhang, C. H. Mak, X. Zou, H.-H. Shen, S.-Y. Leu, H.-Y. Hsu, *J. Mater. Chem. A.* **2018**, *6*, 12842; b) N. K. Tailor, M. Abdi-Jalebi, V. Gupta, H. Hu, M. I. Dar, G. Li, S. Satapathi, *J. Mater. Chem. A.* **2020**, *8*, 21356.
[2] C. Zhang, D.-B. Kuang, W.-Q. Wu, *Small Methods.* **2020**, *4*, 1900662.
[3] a) Z. Shi, A. H. Jayatissa, *Materials.* **2018**, *11*; b) H. S. Jung, N.-G. Park, *Small.* **2015**, *11*, 10.
[4] S. Chang, Z. Bai, H. Zhong, *Adv. Opt. Mater.* **2018**, *6*.
[5] N. Droseros, G. Longo, J. C. Brauer, M. Sessolo, H. J. Bolink, N. Banerji, *ACS Energy Lett.* **2018**, *3*, 1458.
[6] Y.-H. Kim, S. Kim, A. Kakekhani, J. Park, J. Park, Y.-H. Lee, H. Xu, S. Nagane, R. B. Wexler, D.-H. Kim, S. H. Jo, L. Martínez-Sarti, P. Tan, A. Sadhanala, G.-S.u Park, Y.-W. Kim, B. Hu, H. J. Bolink, S. Yoo, R. H. Friend, A. M. Rappe, T.-W. Lee, *Nat. Photonics.* **2021**, *15*, 148.
[7] a) S.-W. Dai, B.-W. Hsu, C.-Y. Chen, C.-A. Lee, H.-Y. Liu, H.-F. Wang, Y.-C. Huang, T.-L. Wu, A. Manikandan, R.-M. Ho, C.-S. Tsao, C.-H. Cheng, Y.-L. Chueh, H.-W. Lin, *Adv. Mater.* **2018**, *30*; b) F. Liu, Y. Zhang, C. Ding, S. Kobayashi, T. Izuishi, N. Nakazawa, T. Toyoda, T. Ohta, S. Hayase, T. Minemoto, K. Yoshino, S. Dai, Q. Shen, *ACS Nano.* **2017**, *11*, 10373.
[8] L. Zhao, Y.-W. Yeh, N. L. Tran, F. Wu, Z. Xiao, R. A. Kerner, Y. L. Lin, G. D. Scholes, N. Yao, B. P. Rand, *ACS Nano.* **2017**, *11*, 3957.
[9] a) E. T. Vickers, T. A. Graham, A. H. Chowdhury, B. Bahrami, B. W. Dreskin, S. Lindley, S. B. Naghadeh, Q. Qiao, J. Z. Zhang, *ACS Energy Lett.* **2018**, *3*, 2931; b) P.o Lu, A. Liu, M. Lu, F. Zhang, S. Sun, M. Liu, Z. Wu, X. Wang, W. Dong, F. Qin, Y. Gao, X. Bai, Y.u Zhang, *Angew. Chem., Int. Ed.* **2024**, *63*, 202317376; c) Y. Jiang, C. Sun, J. Xu, S. Li, M. Cui, X. Fu, Y. Liu, Y. Liu, H. Wan, K. Wei, T. Zhou, W. Zhang, Y. Yang, J. Yang, C. Qin, S. Gao, J. Pan, Y. Liu, S. Hoogland, E. H. Sargent, J. Chen, M. Yuan, *Nature.* **2022**, *612*, 679.
[10] a) L. N. Quan, R. Quintero-Bermudez, O. Voznyy, G. Walters, A. Jain, J. Z. Fan, X. Zheng, Z. Yang, E. H. Sargent, *Adv. Mater.* **2017**, *29*, 1605945; b) S. Wang, A. A. Yousefi Amin, L. Wu, M. Cao, Q. Zhang, T. Ameri, *Small Struct.* **2021**, 2; c) D. N. Dirin, L. Protesescu, D. Trummer, I. V. Kochetygov, S. Yakunin, F. Krumeich, N. P. Stadie, M. V. Kovalenko, *Nano Lett.* **2016**, *16*, 5866; d) S. Liang, M. Zhang, G. M. Biesold, W. Choi, Y. He, Z. Li, D. Shen, Z. Lin, *Adv. Mater.* **2021**, *33*, 2005888; e) W. Cai, Z. Chen, Z. Li, L. Yan, D. Zhang, L. Liu, Q. Xu, Y. Ma, F. Huang, H.-L. Yip, Y. Cao, *ACS Appl. Mater. Interfaces.* **2018**, *10*, 42564.
[11] W. Xu, R. Ji, P. Liu, L.u Cheng, L. Zhu, J.u Zhang, H. Chen, Y. Tong, C. Zhang, Z. Kuang, H. Zhang, J. Lai, K. Wen, P. Yang, N. Wang, W. Huang, J. Wang, *J. Phys. Chem. Lett.* **2020**, *11*, 10348.

[12] Q. Gao, J. Qi, K. Chen, M. Xia, Y. Hu, A. Mei, H. Han, *Adv. Mater.* **2022**, *34*, 2200720.
[13] J.-W. Lee, Y. J.i Choi, J.-M.o Yang, S. Ham, S. K. Jeon, J. Y. Lee, Y.-H. Song, E. K. Ji, D.-H.o Yoon, S. Seo, H. Shin, G. S. Han, H. S. Jung, D. Kim, N.-G. Park, *ACS Nano.* **2017**, *11*, 3311.
[14] J. S. Kim, J.-M. Heo, G.-S.u Park, S.-J.e Woo, C. Cho, H. J. Yun, D.-H. Kim, J. Park, S.-C. Lee, S.-H. Park, E. Yoon, N. C. Greenham, T.-W. Lee, *Nature.* **2022**, *611*, 688.
[15] Y. Sun, Q. Yao, W. Xing, H. Jiang, Y. Li, W. Xiong, W. Zhu, Y. Zheng, *Adv. Sci.* **2023**, *10*, 2205986.
[16] a) F. Deschler, M. Price, S. Pathak, L. E. Klintberg, D.-D. Jarausch, R. Higler, S. Hüttner, T. Leijtens, S. D. Stranks, H. J. Snaith, M. Atatüre, R. T. Phillips, R. H. Friend, *J. Phys. Chem. Lett.* **2014**, *5*, 1421; b) A. O. Murzin, B. V. Stroganov, C. Günnemann, S. B. Hammouda, A. V. Shurukhina, M. S. Lozhkin, A. V. Emeline, Y. V. Kapitonov, *Adv. Opt. Mater.* **2020**, *8*.
[17] Z. Wang, M. Luo, Y. Liu, M. Li, M. Pi, J. Yang, Y. Chen, Z. Zhang, J. Du, D. Zhang, Z. Liu, S. Chen, *Small.* **2021**, *17*, 2101107.
[18] a) D. Jia, J. Chen, M. Yu, J. Liu, E. M. J. Johansson, A. Hagfeldt, X. Zhang, *Small.* **2020**, *16*, 2001772; b) J. Wei, Q. Luo, S. Liang, L. Zhou, P. Chen, Q. Pang, J. Z. Zhang, *J. Phys. Chem. Lett.* **2023**, *14*, 5489; c) M. W. Heindl, T. Kodalle, N. Fehn, L. K. Reb, S. Liu, C. Harder, M. Abdelsamie, L. Eyre, I. D. Sharp, S. V. Roth, P. Müller-Buschbaum, A. Kartouzian, C. M. Sutter-Fella, F. Deschler, *Adv. Opt. Mater.* **2022**, *10*.
[19] J.-H. Kim, Y. R. Kim, B. Park, S. Hong, I.-W. Hwang, J. Kim, S. Kwon, G. Kim, H. Kim, K. Lee, *Small.* **2021**, *17*, 2005608.
[20] J. Zhao, S. Cao, Z. Li, N. Ma, *Chem. Mater.* **2018**, *30*, 6737.
[21] a) C. Liu, Y. Liu, S. Wang, J. Liang, C. Wang, F. Yao, W. Ke, Q. Lin, T.i Wang, C. Tao, G. Fang, *Adv. Opt. Mater.* **2022**, *10*, 2200276; b) Y.u Cao, N. Wang, H.e Tian, J. Guo, Y. Wei, H. Chen, Y. Miao, W. Zou, K. Pan, Y. He, H. Cao, Y. Ke, M. Xu, Y. Wang, M. Yang, K. Du, Z. Fu, D. Kong, D. Dai, Y. Jin, G. Li, H. Li, Q. Peng, J. Wang, W. Huang, *Nature.* **2018**, *562*, 249.
[22] B. Zhu, T. Wang, Z.-K. Tan, *J. Mater. Chem. C.* **2022**, *10*, 10464.
[23] H. Cho, S.u-H. Jeong, M.-H.o Park, Y.-H. Kim, C. Wolf, C.-L. Lee, J. H. Heo, A. Sadhanala, N. Myoung, S. Yoo, S. H. Im, R. H. Friend, T.-W. Lee, *Science.* **2015**, *350*, 1222.
[24] a) G. Shi, Y. Dang, T. Pan, X. Liu, H. Liu, S. Li, L. Zhang, H. Zhao, S. Li, J. Han, R. Tai, Y. Zhu, J. Li, Q. Ji, R. A. Mole, D. Yu, H. Fang, *Phys. Rev. Lett.* **2016**, *117*, 238102; b) L. I. N. Tomé, C. S. R. Sousa, J. R. B. Gomes, O. Ferreira, J. A. P. Coutinho, S. P. Pinho, *RSC Adv.* **2015**, *5*, 15024.
[25] a) C. Zhang, C. Liang, H. Gong, J. Wang, Q.i Song, C. Ji, F. Sun, T. Zhu, X. Huang, Y. Guo, D. Li, F. You, Z. He, *J. Mater. Chem. C.* **2023**, *11*, 11157; b) M. B. Burt, S. G. A. Decker, C. G. Atkins, M. Rowsell, A. Peremans, T. D. Fridgen, *J. Phys. Chem. B.* **2011**, *115*, 11506.
[26] J. M. Richter, M. Abdi-Jalebi, A. Sadhanala, M. Tabachnyk, J. P. H. Rivett, L. M. Pazos-Outón, K. C. Gödel, M. Price, F. Deschler, R. H. Friend, *Nat. Commun.* **2016**, *7*, 13941.
[27] L. Zhang, S. Cui, Q. Guo, C. Ge, Q. Han, Q. Lin, C. Li, X. Zheng, Z. Zhai, L. Wang, Q. Sun, Y. Xu, Y. Liu, X. Tao, *ACS Appl. Mater. Interfaces.* **2020**, *12*, 51616.
[28] a) K.e Chen, Q. Hu, T. Liu, L. Zhao, D. Luo, J. Wu, Y. Zhang, W. Zhang, F. Liu, T. P. Russell, R. Zhu, Q. Gong, *Adv. Mater.* **2016**, *28*, 10718; b) M. Salado, A. D. Jodlowski, C. Roldan-Carmona, G. de Miguel, S. Kazim, M. K. Nazeeruddin, S. Ahmad, *Nano Energy.* **2018**, *50*, 220; c) Y. Hu, J. Shu, X. Zhang, A. Zhao, Y. Liu, R. Li, Y. Di, H. Xu, Z. Gan, *J. Lumin.* **2020**, *219*, 116938; d) P. G. Papagiorgis, A. Manoli, A. Alexiou, P. Karacosta, X. Karagiorgis, G. Papaparaskeva, C. Bernasconi, M. I. Bodnarchuk, M. V. Kovalenko, T. Krasia-Christoforou, G. Itskos, *Front. Chem.* **2019**, *7*, 87.
[29] K.-H. Wang, L.-C. Li, M. Shellaiah, K. W. Sun, *Sci. Rep.* **2017**, *7*, 13643.
[30] a) C. Rehermann, V. Schröder, M. Flatken, F. Ünlü, O. Shargaieva, A. Hoell, A. Merdasa, F. Mathies, S. Mathur, E. L. Unger, *RSC Adv.* **2022**, *12*, 32765; b) K. W. Chou, H. Ullah Khan, M. R. Niazi, B. Yan, R. Li, M. M. Payne, J. E. Anthony, D.-M. Smilgies, A. Amassian, *J. Mater. Chem. C.* **2014**, *2*, 5681; c) D. Barrit, M.-C. Tang, R. Munir, R. Li, K. Zhao, D.-M. Smilgies, *ACS Appl. Mater. Interfaces.* **2022**, *14*, 26315.
[31] S. Pratap, F. Babbe, N. S. Barchi, Z. Yuan, T. Luong, Z. Haber, T.-B. Song, J. L. Slack, C. V. Stan, N. Tamura, C. M. Sutter-Fella, P. Müller-Buschbaum, *Nat. Commun.* **2021**, *12*, 5624.
[32] a) K. Mantulnikovs, A. Glushkova, M. Kollár, L. Forró, E. Horváth, A. Sienkiewicz, *ACS Appl. Electron. Mater.* **2019**, *1*, 2007; b) Y. D. Glinka, R. Cai, X. Gao, D. Wu, R. Chen, X. W. Sun, *AIP Adv.* **2020**, *10*; c) P. Kumar, C. Muthu, C. Vijayakumar, K. S. Narayan, *J. Phys. Chem. C.* **2016**, *120*, 18333; d) R. Brenes, C. Eames, V. Bulović, M. S. Islam, S. D. Stranks, *Adv. Mater.* **2018**, *30*, 1706208.
[33] Y. Dang, Y. Liu, Y. Sun, D. Yuan, X. Liu, W. Lu, G. Liu, H. Xia, X. Tao, *CrystEngComm.* **2015**, *17*, 665.
[34] a) S.-H. Chin, J. W. Choi, H. C. Woo, J. H. Kim, H. S. Lee, C.-L. Lee, *Nanoscale.* **2019**, *11*, 5861; b) B. Li, B. Chang, L. Pan, Z. Li, L. Fu, Z. He, L. Yin, *ACS Energy Lett.* **2020**, *5*, 3752; c) F. Wang, D. Duan, Y. Sun, T. Wang, G. Yang, Q. Li, Y. Li, X. Liang, X. Zhou, X. Sun, J. Ma, J. Xiang, J. Zhu, Q. Zhu, K. Zhou, H. Lin, Y. Shi, G. Li, H. Hu, *Nano Energy.* **2024**, *125*, 109549; d) H. Jiang, J. Feng, H. Zhao, G. Li, G. Yin, Y. Han, F. Yan, Z. Liu, S. F. Liu, *Adv. Sci.* **2018**, *5*, 1801117.
[35] a) J. Cao, Q. Wang, W. Li, C. Yan, X. Zeng, Y. Gao, X. Zheng, J. Lu, W. Yang, *J. Colloid Interface Sci.* **2022**, *626*, 591; b) E. S. Parrott, J. B. Patel, A.-A. Haghighirad, H. J. Snaith, M. B. Johnston, L. M. Herz, *Nanoscale.* **2019**, *11*, 14276.
[36] F. Qin, Z. Wang, Z. L. Wang, *ACS Nano.* **2016**, *10*, 9787.
[37] a) S. Ghosh, P. Kar, *Inorg. Chem.* **2022**, *61*, 10079; b) A. K. Sharma, P. Bansal, G. K. Nim, P. Kar, *Part. Part. Syst. Charact.* **2019**, *36*, 1900328.
[38] G. Mannino, I. Deretzis, E. Smecca, A. La Magna, A. Alberti, D. Ceratti, D. Cahen, *J. Phys. Chem. Lett.* **2020**, *11*, 2490.
[39] U. Holzwarth, N. Gibson, *Nat. Nanotechnol.* **2011**, *6*, 534.
[40] S. A. Hassanzadeh-Tabrizi, *J. Alloys Compd.* **2023**, *968*, 171914.
[41] a) P. Khoram, S. Brittman, W. I. Dzik, J. N. H. Reek, E. C. Garnett, *J. Phys. Chem. C.* **2016**, *120*, 6475; b) Q. Liao, K. Hu, H. Zhang, X. Wang, J. Yao, H. Fu, *Adv. Mater.* **2015**, *27*, 3405; c) C. Li, F. Chen, K. Wang, Q. Yao, J. Zhang, Q. Zhao, Q. Huang, H. Zhu, J. Ding, *J. Mater. Chem. C.* **2022**, *10*, 14580.
[42] a) G. Li, M. Price, F. Deschler, *APL Mater.* **2016**, *4*; b) K. Wang, S. Wang, S. Xiao, Q. Song, *Adv. Opt. Mater.* **2018**, *6*, 1800278; c) N. Feng, M. Lu, S. Sun, A. Liu, X. Chai, X. Bai, J. Hu, Y. Zhang, *Laser Photonics Rev.* **2023**, *17*.
[43] L. Lei, Q. Dong, K. Gundogdu, F. So, *Adv. Funct. Mater.* **2021**, *31*.
[44] Y. J. Yoon, Y. S. Shin, C. B. Park, J. G. Son, J. W. Kim, H. S. Kim, W. Lee, J. Heo, G.-H. Kim, J. Y. Kim, *Nanoscale.* **2020**, *12*, 21695.
[45] K. Zheng, Q. Zhu, M. Abdellah, M. E. Messing, W. Zhang, A. Generalov, Y. Niu, L. Ribaud, S. E. Canton, T. Pullerits, *J. Phys. Chem. Lett.* **2015**, *6*, 2969.
[46] S. Lan, Y. Peng, H. Shen, S. Wang, J. Ren, Z. Zheng, W. Liu, D. Li, *Laser Photonics Rev.* **2021**, *15*.
[47] H. Cao, *Waves Random Media.* **2003**, *13*, R1.
[48] a) A. Liu, G. Guan, X. Chai, N. Feng, M. Lu, X. Bai, Y. Zhang, *Laser Photonics Rev.* **2022**, *16*; b) J. Moon, Y. Mehta, K. Gundogdu, F. So, Q. Gu, *Adv. Mater.* **2024**, *36*, 2211284.
[49] A. G. Barrette, *Dissertation*, North Carolina State University, Raleigh **2018**.
[50] S. Sidhik, W. Li, M. H. K. Samani, H. Zhang, Y. Wang, J. Hoffman, A. K. Fehr, M. S. Wong, C. Katan, J. Even, A. B. Marciel, M. G. Kanatzidis, J.-C. Blancon, A. D. Mohite, *Adv. Mater.* **2021**, *33*, 2007176.